Inorganic Chemistry
Article
Cite This: Inorg. Chem. 2020, 59, 1227−1233
pubs.acs.org/IC

Os^{4+} Instability in the Pyrochlore Structure: $Tl_{2-x}Bi_xOs_2O_{7-y}$

Elizabeth Sobalvarro Converse,[†] Jun Li,[†] Daniel Haskel,[‡] Patrick G. LaBarre,[§] Arthur P. Ramirez,[§] and M. A. Subramanian*[,†]

[†]Department of Chemistry. Oregon State University, Corvallis, Oregon 97331, United States
[‡]Advanced Photon Source, Argonne National Laboratory, Lemont, Illinois 60439, United States
[§]Department of Physics, University of California, Santa Cruz, California 95064, United States

Supporting Information

ABSTRACT: Osmium-containing oxides are rare due to the difficulty in stabilizing complex structures with a fixed stoichiometry and metastability of the phases. Bismuth-substituted thallium osmate pyrochlore samples, $Tl_{2-x}Bi_xOs_2O_{7-y}$, were synthesized using solid-state reactions where the solubility limit was found to be approximately x = 1.4. Members of this solid solution were characterized by their structural, electronic, magnetic, and thermal properties to understand the influence of Bi^{3+} substitution on the ground state. The Os-containing pyrochlores crystallize in the ideal cubic pyrochlore structure ($Fd\bar{3}m$), and the lattice parameter a was found to slightly increase as a function of Bi content. A possible interplay between structure and cation valence states was explored using both neutron powder diffraction and X-ray absorption spectroscopy, suggesting that a combination of Os^{4+}/Os^{5+} and Tl^{1+}/Tl^{3+} mixed valency throughout the solid solution allows for the stabilization of the pyrochlore structure. The system is metallic for the entire solid solution and predominantly exhibits temperature-independent paramagnetism. Specific heat measurements show an enhanced Sommerfeld coefficient, a possible flat-band signature. This system gave insight into the bonding preferences of Os, indicating a dependence on high oxidation states and mixed valence for the stability of complex structures.

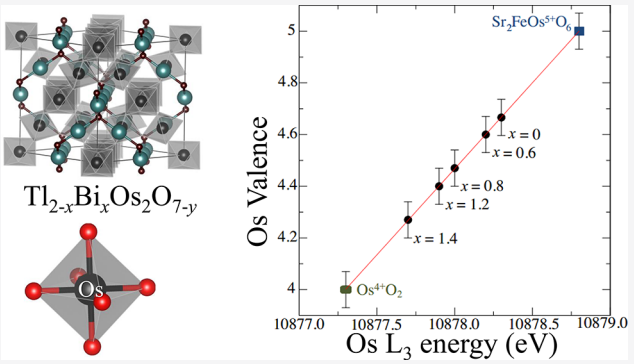

INTRODUCTION

Materials that crystallize in the pyrochlore structure have been extensively studied for their promising properties in a variety of applications. The ideal pyrochlore structure crystallizes in the $Fd\bar{3}m$ cubic space group and has the formula $A_2M_2O_6O'$ which can accept vacancies at both the A and O′ sites. The structure is described as two interpenetrating networks of corner-shared MO_6 octahedra and A_2O' chains.[1] Pyrochlores containing a 5d transition metal are of interest due to their spatially extended 5d orbitals, modest electron correlations, large spin−orbital coupling, and a propensity to form flat bands, a manifestation of frustrated hopping (Figure 1). These effects give rise to exotic physical properties such as superconductivity[2] and potential topologically protected states of matter.[3]

Osmate compounds in general have also been shown to exhibit interesting properties such as a metal−insulator transition[4] and a potential quantum spin liquid state.[5] However, few osmate oxides are known due to the difficulty in stabilizing these compounds. In fact, the rare-earth osmate pyrochlores reported to exist[6] have not to date been reproduced or characterized. The literature is limited regarding the structures of the known osmate oxides which have been stabilized, including the driving force of their stability.

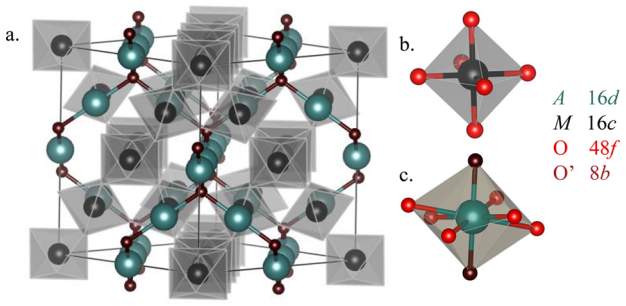

Figure 1. (a) The pyrochlore structure shown highlighting the two interpenetrating networks of A_2O' chains and MO_6 octahedra. (b) Coordination at the M site showing the MO_6 octahedra. (c) Coordination at the A site with six long A−O bonds and two short A−O′ bonds forming a distorted cube environment.

Among the osmate compounds, bismuth osmate with an equal Bi to Os mole ratio was suspected to belong to the $KSbO_3$ structure type.[7] This was proven through a later study involving neutron diffraction experiments and was found to be

Received: October 3, 2019
Published: January 7, 2020

DOI: 10.1021/acs.inorgchem.9b02939
Inorg. Chem. 2020, 59, 1227−1233

a slightly bismuth deficient material with the final formula of $Bi_{2.93}Os_3O_{11}$[8,9] or $Bi_{1.95}Os_2O_{7.33}$. Recently $Bi_2Ir_2O_{6.815}$ was studied as a potential topological insulator.[10] While $Bi_2Ir_2O_{6.815}$ forms readily, the bismuth osmate pyrochlore $Bi_2Os_2O_{7-y}$ does not form even under high pressure, instead crystallizing in the $KSbO_3$ structure type.

Importantly, the thallium analogue $Tl_2Os_2O_{7-y}$ is known to exist as an anion-deficient pyrochlore[11] and forms readily at relatively low temperatures in comparison to other precious-metal pyrochlores. This previous study with synthesis at ambient pressure concluded that charge compensation from the missing O anions arises entirely from a mixture of Tl^+ and Tl^{3+}, with Os remaining in the +4 oxidation state, but this was not investigated beyond neutron powder diffraction. However, under high pressure it was found that this system can exist as stoichiometric.[12] This indicates that under pressure a change in the structure occurs which allows for the stoichiometry to be fixed and mixed valency is no longer necessary. While it is possible for an osmate oxide to stabilize in the +4 oxidation state, these compounds are generally metastable. This is best shown through OsO_2, which will quickly oxidize to OsO_4 when it is heated in air. It is reasonable then to suspect that all Os present in the sample may not be Os^{4+} in the case of the $Tl_2Os_2O_{7-y}$ prepared at ambient pressure.

The present work aims to determine the solubility limit of Bi^{3+} in the osmate pyrochlore structure to help elucidate the bonding preferences of Os. This is achieved through the investigation of a solid solution between the known $Tl_2Os_2O_{7-y}$ and unknown $Bi_2Os_2O_{7-y}$. Here, we offer detailed neutron refinements and X-ray absorption measurements for select members of this solid solution to understand the stability and crystal structure of these pyrochlore samples. In addition, thermodynamic and transport measurements were performed to explore the collective electronic behavior in the series and its dependence on Bi^{3+} incorporation.

EXPERIMENTAL SECTION

Stoichiometric amounts of Bi_2O_3 (Sigma-Aldrich, 99.9%), OsO_2 (synthesized from Os metal), and 25 mol % excess Tl_2O_3 (Johnson Matthey, 99.999%) were ground together using an agate mortar and pestle and pelletized before being placed into a quartz tube and sealed under vacuum at 10^{-4} Torr. The sample in the quartz ampule was heated between 500 and 650 °C for 12 h with intermittent grinding and resealing until phase pure. Polycrystalline samples were pressed into bars at 0.5 metric ton and placed into sealed in quartz tubes for sintering to a density of about 70%. The authors stress the importance of safely handling compounds containing thallium and osmium according to their SDS due to toxicity.

Phase purity and lattice parameters were determined using a Rigaku Miniflex X-ray diffractometer (Cu Kα radiation) with a graphite monochromator on the diffracted beam. Le Bail fitting was performed using NaCl as an internal standard for accurate lattice parameter determination. Neutron diffraction data were collected to perform structural characterization on the samples. Time of flight (TOF) neutron diffraction data were collected at the Oak Ridge National Laboratory (ORNL) Nanoscale-Ordered Materials Diffractometer (NOMAD) BL-1B SNS beamline due to the small sample size. Rietveld analysis was performed using the General Structural Analysis System (GSAS) EXPGUI interface.[13]

X-ray absorption spectroscopy (XAS) measurements were carried out at beamline 4-ID-D of the Advanced Photon Source (APS) across Os $L_{2,3}$ absorption edges to help confirm the average oxidation state of the osmium in this series. Using this technique, eight samples from the $Tl_{2-x}Bi_xOs_2O_{7-y}$ solid solution were measured ($0 \leq x \leq 1.4$). A pair of toroidal and flat Pd mirrors at 3.1 mrad incidence angle was used to reject higher energy undulator harmonics. Additionally, the second crystal of a double-crystal Si (111) monochromator was detuned (20% reduction in fundamental intensity) to provide additional harmonic rejection. Reference samples for valence determination included $Os^{4+}O_2$ and $Sr_2FeOs^{5+}O_6$.[14]

The Seebeck coefficient and electrical conductivity data (350−500 K) were collected on an ULVAC ZEM-3 instrument using a helium atmosphere. Magnetization measurements (2−300 K) were performed using a Quantum Design MPMS instrument. Resistivity and specific heat measurements (2−90 K) were obtained using a Quantum Design PPMS instrument. The low-temperature resistivity measurements were performed on pressed bars of polycrystalline material, and electrical contact was made with Ag-epoxy. The specific heat measurements were made on pieces from the same bars using the PPMS-based relaxation method, and thermal coupling was provided by a silicone grease bond. Despite the polycrystalline nature of the samples, thermal equilibration was facilitated by the conduction electrons and good thermal contact was indicated by the PPMS coupling parameter, which was above 90% for $x = 0$, 1 samples. For $x = 0.5$, the coupling was too low and the associated data are not reported.

RESULTS AND DISCUSSION

Structural Analysis of $Tl_{2-x}Bi_xOs_2O_{7-y}$. All $Tl_{2-x}Bi_xOs_2O_{7-y}$ samples were determined to be nearly phase pure (Figure 2) with trace amounts of OsO_2 or Os metal as a

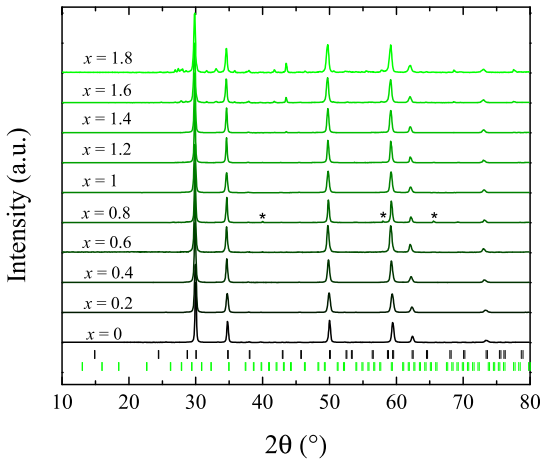

Figure 2. X-ray powder diffraction patterns for $Tl_{2-x}Bi_xOs_2O_{7-y}$. Black tick marks (top) are representative of the pyrochlore phase, while the green tick marks (bottom) indicate the peak positions of $Bi_3Os_3O_{11}$ with the $KSbO_3$-type structure. Peaks marked with asterisks are due to small Os impurities.

direct result of Tl volatility. At $x = 1.4$ small peaks associated with $Bi_3Os_3O_{11}$ appear, marking the solubility limit; the lack of superlattice peaks indicates that Tl, Bi, and vacancies within the pyrochlore structure are disordered.[1] X-ray analyses show that all samples within the solid solution crystallize in the ideal cubic pyrochlore structure ($Fd\bar{3}m$). If Tl^{3+} were replaced solely by Bi^{3+}, the lattice would expand due to the difference in ionic radii: 0.98 and 1.17 Å, respectively.[15] However, the variation of the lattice parameters with increasing Bi^{3+} content does not follow Vegard's law strictly, indicating a more complex substitution mechanism likely due to the mixed valence of Os and/or Tl (Figure 3). In the same manner, O′ site vacancies can contribute to the small level of scattering in the lattice parameters in Figure 3. With slightly more or less oxygen content, it is possible to increase or decrease the lattice parameter a. To further investigate the structural changes observed with the addition of Bi^{3+} to this system, neutron

DOI: 10.1021/acs.inorgchem.9b02939
Inorg. Chem. 2020, 59, 1227−1233

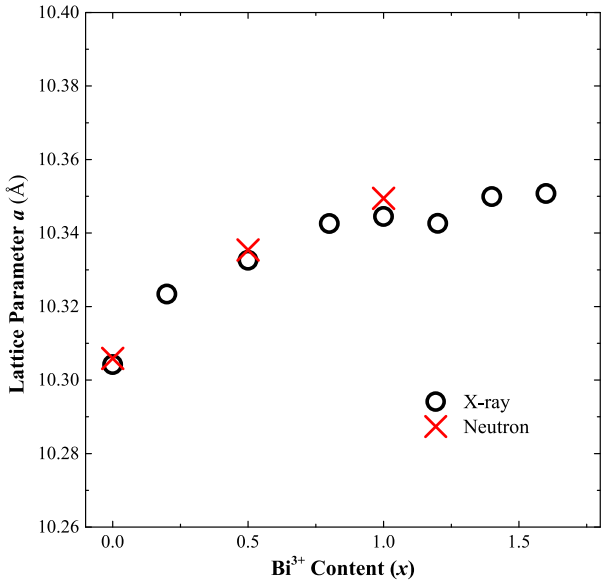

Figure 3. Dependence of the unit cell edge upon the nominal Bi content for the $Tl_{2-x}Bi_xOs_2O_{7-y}$ solid solution. The unit cell expands until the solid solution ends around x = 1.4, where the lattice parameter a stops increasing systematically and $Bi_3Os_3O_{11}$ impurities begin to form.

diffraction analysis was performed on three $Tl_{2-x}Bi_xOs_2O_{7-y}$ samples (x = 0, 0.5, 1.0).

The neutron data of the x = 0, 0.5, and 1 samples were analyzed using the Rietveld method to refine the structure. Using conventional X-ray diffraction, it is not possible to separate Tl and Bi due to a lack of contrast. The neutron scattering lengths are again similar, with 8.776 fm for Tl and 8.532 fm for Bi, rendering them indistinguishable from one another. However, due to the low-temperature synthesis of these samples Bi will not volatilize while Tl will, as made evident by the higher melting point of Bi in comparison to Tl. In addition, there were no observable Bi impurities in these samples, allowing for the Bi content in the samples to be fixed at the nominal composition. All three samples crystallize in the ideal pyrochlore structure, with no evidence of cation ordering or displacement at the A or O′ sites.

The x = 0 sample follows precedent, exhibiting only anion vacancies in the structure; however, the larger than average atomic displacement parameter (ADP) at the A site indicates a possibility of local distortion (Figure 4). This local distortion is

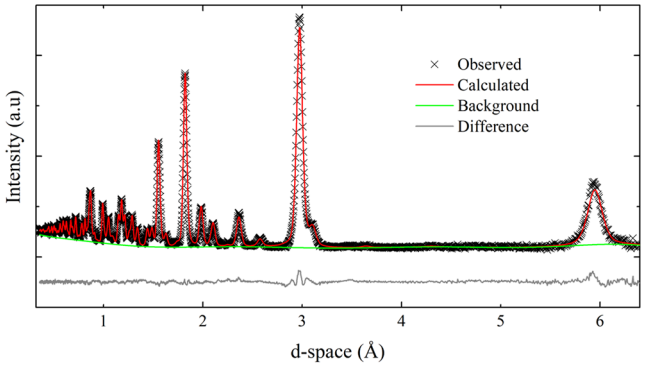

Figure 4. Rietveld structural refinement of $Tl_2Os_2O_{6.639(7)}$ shown for a selected high-resolution bank.

known to occur when a lone pair is present in the structure, implying the presence of Tl^+. The magnitude of displacement caused by the lone pair was small enough to be modeled using anisotropic ADPs rather than a static displacement. The parent compound exhibited no A site vacancies but displayed significant O′ site vacancies, (Table 1). The observed O′ vacancies would be necessary to accommodate the lone pair from Tl^+, showing further evidence for this stoichiometry.[16] However, this does not remove the possibility of Os mixed valence in this structure; diffraction data alone will not be able to elucidate this situation.

Neutron analysis for the new compositions, x = 0.5 and x = 1, reveals A site vacancies which are attributed to Tl due to the observed experimental volatilization (Figure 5). The O′ site vacancies and larger ADPs at the A site were observed, again indicating the presence of a lone pair. This, however, does not reveal much about the structure, as both Bi^{3+} and Tl^+ have lone pairs and are possible in this structure. The A site was modeled at all possible Wykoff positions as allowed by symmetry, but the refinement was only stable when the A site cations were placed at the ideal position 16d. As Bi and Tl share a site, it was not appropriate to describe the ADPs of the A site cations using anisotropic U values; however, they are well described using slightly larger isotropic U values. The possibility of Tl^+ combined with the probable mixed valence at the Os site warrants additional analysis.

Nuclear density Fourier maps were used as a complementary method of structure determination in order to verify the final structural models. Two different Fourier maps, the observed (F_{obs}) and difference maps, were calculated for this purpose. The nuclear density for all three samples (x = 0, 0.5, and 1) using both Fourier maps resulted in the ideal pyrochlore structure. The only anomaly in the nuclear density was found to be present at the M site where Os resides. This deviation can be observed when mixed valence is present due to the varying ionic radii, leading to further evidence of Os mixed valence throughout the solid solution. Using XAS measurements, the Os valence states can be determined in order to further describe the structure.

XAS measurements of the Os L_2 and L_3 absorption edges ($2p_{1/2,3/2} \rightarrow 5d$ resonant excitation) were used to find the average Os oxidation states in eight samples within the solid solution, $0 \leq x \leq 1.4$ (Figure 6). The enhanced absorption right above the leading edge, usually referred to as "white line", is a result of a large density of empty 5d states near the Fermi level. The Os L_2 and L_3 white lines shift from higher to lower energy, indicating a systematic reduction of Os^{5+} to Os^{4+} with increasing Bi^{3+} content (Figure 7). Linear interpolation of the edge energy values into those of the +4 and +5 reference compounds yields valences of +4.66(7) and +4.27(7) for the x = 0 and x = 1.4 samples, respectively. The Rietveld refinement results corroborate this systematic reduction by revealing an increasing Os−O bond length with increasing Bi^{3+} content. This expansion is expected due to the differences in ionic radii between Os^{4+} and Os^{5+}: 0.63 and 0.575, respectively.[15] Bond valence sum (BVS) calculations[17] were performed on the OsO_6 octahedra to track the change in oxidation state. The bond valences when the BVS parameter for Os^{5+} was used were found to be 4.77, 4.71, and 4.65 for x = 0, 0.5, and 1, respectively, consistent with the XAS results within error. These values highlight that the bond distances between the mixed-valent Os and O in the octahedra are decreasing, as

DOI: 10.1021/acs.inorgchem.9b02939
Inorg. Chem. 2020, 59, 1227−1233

Table 1. Summary of Neutron Structure Refinements for the $Tl_{2-x}Bi_xOs_2O_{7-y}$ Phases

nominal Bi^{3+} content	$x = 0$	$x = 0.5$	$x = 1$
refined formula	$Tl_2Os_2O_{6.639(7)}$	$Tl_{1.43(2)}Bi_{0.5}Os_2O_{6.579(5)}$	$Tl_{0.968(2)}BiOs_2O_{6.608(5)}$
wRp (%)[a]	4.10	2.68	3.36
a (Å)	10.3038(1)	10.3349(1)	10.3487(1)
O position (x)[b]	0.31885(6)	0.31857(4)	0.31914(4)
O′ occ	0.634(7)	0.579(5)	0.608(5)
Tl A site occ	1	0.715(2)	0.484(2)
Bi^{3+} A site occ[c]		0.25	0.5
O U_{iso}[d]	0.0115(2)	0.00852(2)	0.00804(2)
O′ U_{iso}	0.0106(5)	0.0144(6)	0.0151(5)
A site U_{iso}	0.0116(1)	0.0099(1)	0.0133(1)
Os U_{iso}	0.00278(6)	0.00263(3)	0.00131(2)
Os−O (×6)	1.9547(3)	1.9596(2)	1.9644(2)
Os oxidation state	4.66[e]	4.6[f]	4.47[e]

[a]Statistics for the selected high-resolution bank. [b]Atomic position of O is at (x, $^1/_8$, $^1/_8$). [c]occ denotes occupancy which was not refined. [d]Anisotropic U values are provided in the CIF files. [e]Values obtained through XAS measurements. [f]Value estimated on the basis of the experimental XAS data.

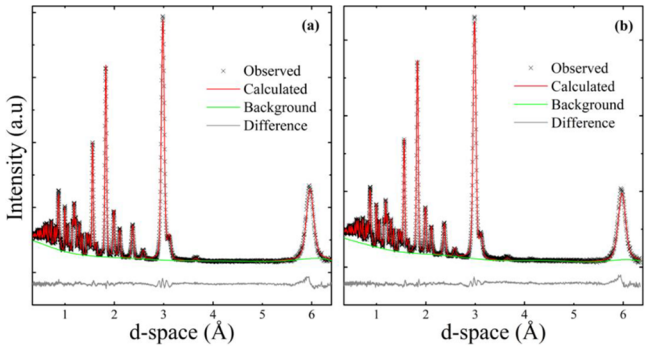

Figure 5. Neutron structural refinement shown for the selected high-resolution bank for samples within the $Tl_{2-x}Bi_xOs_2O_{7-y}$ solid solution: $x = 0.5$ (a) and $x = 1$ (b).

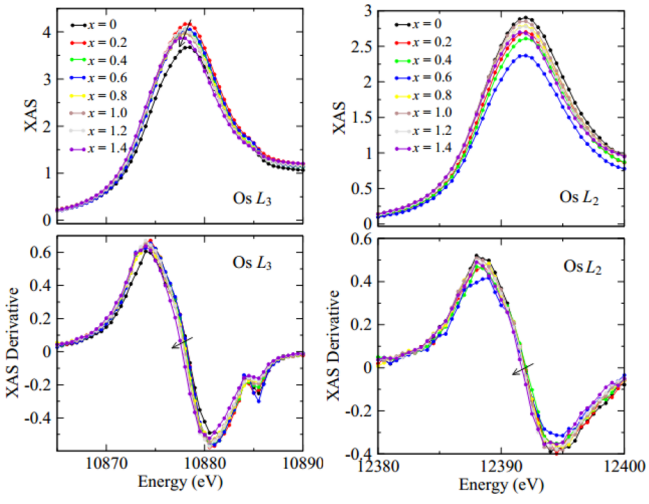

Figure 6. XAS measurements of the $Tl_{2-x}Bi_xOs_2O_{7-y}$ samples at the Os L_2 and L_3 absorption edges.

expected for a reduction in charge. The bond valence confirms the systematic reduction of Os with increasing Bi content.

The average oxidation states of the $Tl_{2-x}Bi_xOs_2O_{7-y}$ samples as determined by XAS measurements were revealed to be 4.67(7), 4.60(7), and 4.47(7) for the $x = 0$, 0.5, and 1 samples, respectively (Figure 8). All additional Os valence states determined have been reported in Figure S1 in the Supporting

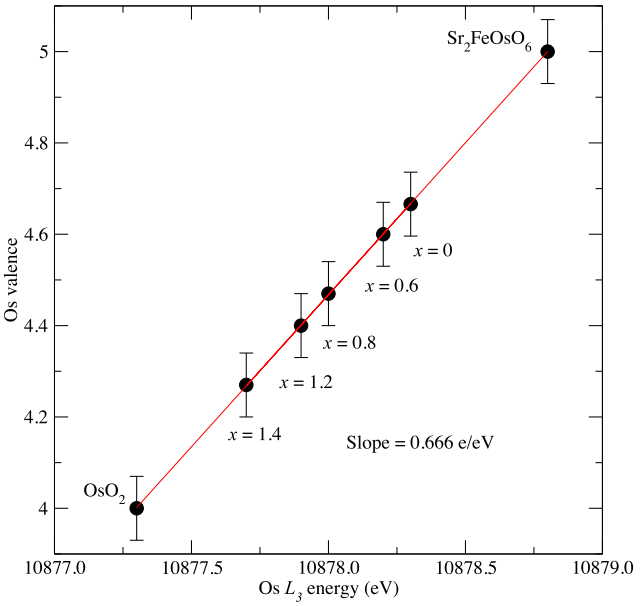

Figure 7. Os valence as a function of the measured Os L_3 edge energy obtained by XAS for the $Tl_{2-x}Bi_xOs_2O_{7-y}$ samples.

Information. The oxidation states obtained from XAS, combined with the refined neutron occupancies, allow for the determination of Tl^+, Tl^{3+}, Os^{4+}, and Os^{5+} stoichiometries, giving rise to the final determined formulas found in Table 2. While these formulas only show a simplification to point charges from average oxidation states, it illustrates the systematic reduction of Os^{5+} to Os^{4+} with addition of Bi^{3+}. It is also evident that Tl^+ content is decreasing in the system as a function of Bi^{3+}. The formulas shown are derived from a combination of the refined neutron occupancies and XAS data, allowing for an overall stoichiometry solution. The increase in lattice parameters validates the obtained average stoichiometries for these systems. While a decrease in the amount of Tl^+ in the structure should yield a lattice contraction, the substitution of Bi^{3+} for Tl^{3+} and a reduction of Os^{5+} to Os^{4+} contributes to an overall lattice expansion of about 0.44% from $x = 0$ to $x = 1$, resulting in a change much smaller than expected for a simple cation substitution. Finally, the effect of the anion vacancies can also contribute to the overall lattice

DOI: 10.1021/acs.inorgchem.9b02939
Inorg. Chem. 2020, 59, 1227−1233

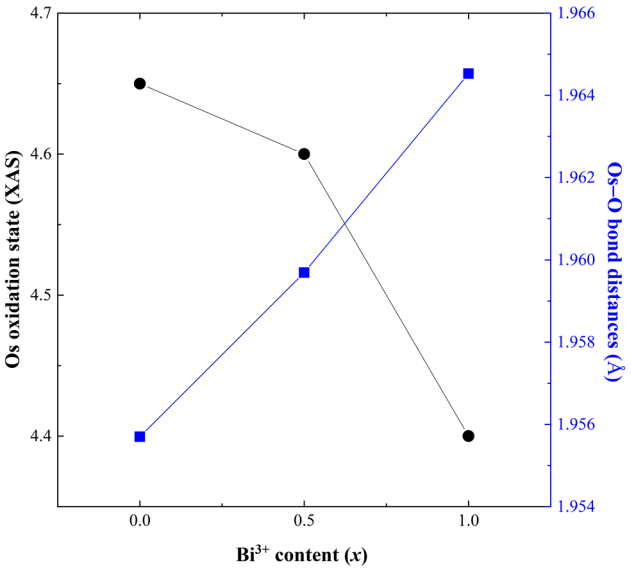

Figure 8. Osmium oxidation state (circles) and Os−O bond lengths (squares), as obtained from XAS measurements and neutron refinements, respectively, vs x for the $Tl_{2-x}Bi_xOs_2O_{7-y}$ system.

change. While oxygen content variation during our syntheses was minimal due to the use of sealed tubes, variation of the oxygen content in the crystal structure could contribute to the lattice expansion/contraction. The effect of oxygen content on the lattice parameters in this system seems to be minor compared to the $Tl^+/Tl^{3+}/Bi^{3+}$ ionic radii differences but may play a role in the nonlinear increase of the lattice between x = 0.5 and 1.

While a pure bismuth osmate pyrochlore was not stabilized, this $(Tl,Bi)Os_2O_7$ system gave insight into the bonding preferences of Os in more complex structures. Osmium in the system studied prefers to exist in a mixed valence state, following precedent.[5,8,9,18,19] A high level of mixed valence would be difficult to stabilize in a pyrochlore containing only Bi^{3+} at the A site, causing the instability of the single-phase bismuth osmate pyrochlore. Rather than adopting the pyrochlore structure, bismuth osmate will instead preferentially form the $KSbO_3$ structure type ($Bi_3Os_3O_{11}$), which allows for Os to remain mixed valent. This phenomenon can help to explain why rare-earth osmates are difficult to synthesize, showing reaction times of weeks in the literature.[6] Rare-earth osmate pyrochlores were attempted following this published procedure; however, none of our syntheses resulted in pyrochlore formation. To our knowledge, no rare-earth osmate pyrochlores have been synthesized since this report, showing the difficulty of reproducing this result. While $Os^{4+}O_2$ can be stabilized, this process must be controlled by adding in stoichiometric amounts of O_2 gas in order to not further oxidize the Os to $Os^{8+}O_4$. Overall it is clear that, under standard conditions, Os prefers higher oxidation states. This shows that the driving force for stabilizing complex structure types containing Os relies on the presence of both mixed-valence and higher oxidation states at ambient pressure.

Resistivity and Transport Properties. Resistivity, $\rho(T)$, and thermopower, $S(T)$, measurements were measured in both high- (>300 K) and low-temperature (<300 K) ranges. The $\rho(T)$ value at high temperature showed typical metallic behavior and was only observed in a limited range (300−475 K) due to the volatility and reactivity of Tl and Os at high temperatures. The $\rho(T)$ data shown in Figure 9a reveal

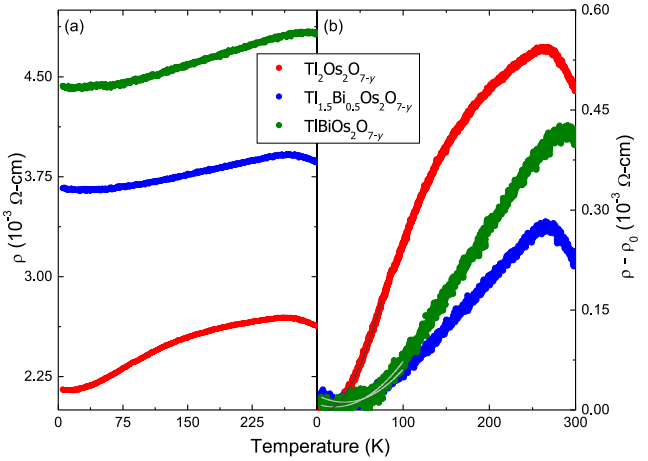

Figure 9. (a) Low-temperature resistivity as collected using a quantum design physical properties measurement system. (b) Resistivity at 0 K (ρ_0) subtracted from the measured resistivity (ρ) vs T for the $Tl_{2-x}Bi_xOs_2O_{7-y}$ samples.

metallic behavior at all temperatures below 230 K, albeit with temperature-dependent changes that are smaller than the T = 0 value (ρ_0), implying a high degree of impurity scattering. In Figure 9b, ρ_0 is subtracted from $\rho(T)$, the result of which is fitted to a quadratic formula in order to extract a Fermi liquid T^2 coefficient. We find for this coefficient A = 0.034, 0.011, and 0.011 $\mu\Omega$ cm/K^2 for x = 0, 0.5, and 1, respectively, which will be compared to the specific heat, $C(T)$, Sommerfeld coefficient below.

Magnetism. The susceptibility, $\chi(T)$, for the three compounds presented in Figure 10a shows three different contributions. First, for T < 20 K, one sees a Curie tail which can be ascribed to less than 1% of impurity spins. Second, all three data sets seem to be dominated by a temperature-independent term. We note that the nominal valence here is +4, which, like Ir^{5+}, can be expected to exhibit van Vleck temperature-independent paramagnetism. The Fermi liquid behavior implied by the A term in $\rho(T)$ would also yield a Pauli temperature-independent term, discussed below. The third contribution to $\chi(T)$ is a weak temperature-dependent

Table 2. Formulas for the $Tl_{2-x}Bi_xOs_2O_{7-y}$ Solid Solution Described as Point Charges Using a Combination of XAS and Neutron Structural Refinement[a]

x	refined formula	final formula
0	$Tl_2Os_2O_6O'_{0.639(7)}$	$(Tl^+_{0.98}Tl^{3+}_{1.02})(Os^{4+}_{0.68}Os^{5+}_{1.32})O_6O'_{0.639(7)}$
0.5	$Tl_{1.43(2)}Bi_{0.5}Os_2O_6O'_{0.579(5)}$	$(Tl^+_{0.92}Tl^{3+}_{0.51})Bi_{0.5}(Os^{4+}_{0.8}Os^{5+}_{1.2})O_6O'_{0.579(5)}$
1	$Tl_{0.968(2)}BiOs_2O_6O'_{0.608(5)}$	$(Tl^+_{0.81}Tl^{3+}_{0.15})Bi(Os^{4+}_{1.06}Os^{5+}_{0.94})O_6O'_{0.608(5)}$

[a]Bi occupancies are fixed. XAS values for Os valence, from which Tl^+/Tl^{3+} and Os^{4+}/Os^{5+} amounts are calculated, have an uncertainty of ±0.07.

DOI: 10.1021/acs.inorgchem.9b02939
Inorg. Chem. 2020, 59, 1227−1233

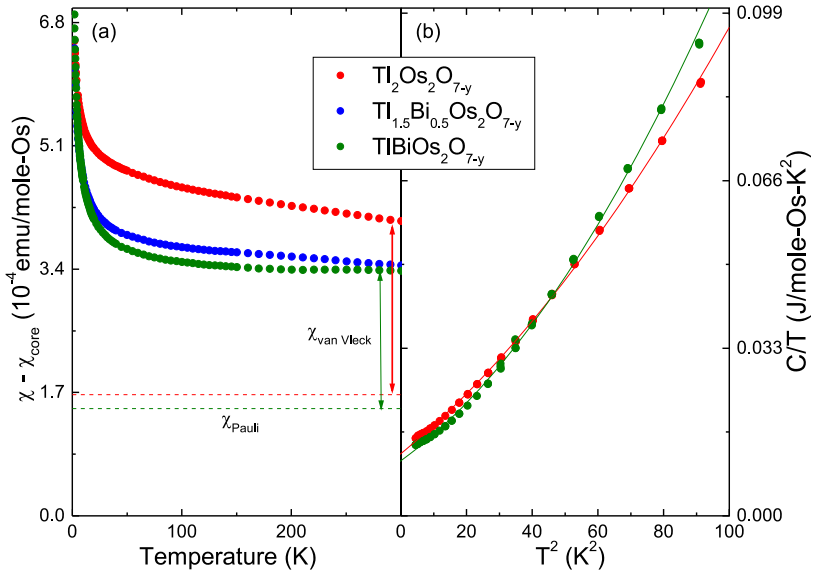

Figure 10. (a) Magnetic susceptibility data along with derived values of $\chi_{van\ Vleck}$ and χ_{Pauli} as derived from the $C(T)$ linear term coefficient. (b) The specific heat (C/T) of $Tl_{2-x}Bi_xOs_2O_{7-y}$ samples. The solid lines are least-squares fits of C/T to a quadratic polynomial in T^2. Thus, the fit captures terms in C varying as T, T^3 and T^5 with coefficients to these terms respectively being 0.0122 (0.0108), 5.28×10^{-4} (4.675×10^{-4}), and 3.12×10^{-6} (5.14×10^{-6}) for $x = 0$.

term that is greatest for $x = 0$ and absent for $x = 1$. Analyzing this as a contribution independent of the constant $\chi(T)$ terms yields a density of $S = 1/2$ spins in the 2% range for $x = 0$. Thus, the χ(T) data point to two distinct types of impurity spins.

Specific Heat. We were able to obtain specific heat, $C(T)$, data for $x = 0$ and 1, shown in Figure 10b as C/T vs T^2. The accuracy of the specific heat data is most likely comparable to that of copper, where measurements on different samples using a similar apparatus yielded uncertainties in the range of 2%, which is less than the size of our data points.[20] Fitting these data to $C(T)/T = \gamma + \beta T^2$, only over the lowest temperature range, 2−4 K, allows the extraction of the coefficient γ and the Debye lattice contribution β, and we find $\gamma = 0.0122$ and 0.0108 J/(mol K) for $x = 0$ and 1, respectively. The β values have little physical significance, given the small range over which the data are fitted, though the deviation from Debye behavior above 4 K may be of future significance. Assuming that the γ term is due to conduction electrons, we can compare it with the A values for two of our compounds and place this system on the Kadowaki−Woods plot used to interpret mass enhancement in heavy Fermion compounds.[21] We find that A is larger than expected for heavy Fermions, which implies that the presence of scattering is unrelated to a Fermi liquid picture and perhaps is related to the defects indicated by the Curie tail in $\chi(T)$. Extending the Fermi liquid analysis, we can estimate the Pauli contribution (χ_{Pauli}) to the susceptibility, via $\gamma = 1/3(\pi k_B/\mu_B)^2\chi_{Pauli}$, for $x = 0$ and 1. In Figure 10a, we show these derived values compared to the measured $\chi(T)$, the difference being an inferred van Vleck contribution in the range of $\sim 2 \times 10^{-4}$ emu/mol, which is comparable to the values found for Ir^{5+} compounds. Given the admittedly large uncertainties associated with the assumptions made here, we nevertheless find a remarkable degree of consistency among resistivity, susceptibility, and specific heat leading to the thallium osmate pyrochlores falling into a new class of Fermi liquids but with no obvious flat band effects.

CONCLUSIONS

The $Tl_{2-x}Bi_xOs_2O_{7-y}$ samples were successfully synthesized up to $x \approx 1.4$, showing the solubility limit for Bi^{3+} in the osmate pyrochlore structure. A combination of XAS and neutron diffraction structure refinement revealed that a combination of Tl^+/Tl^{3+} and Os^{4+}/Os^{5+} mixed valence stabilizes the pyrochlore structure. As Bi^{3+} was introduced to the system, Os was further reduced until the pyrochlore was no longer the preferred phase, and a new phase was formed with the $KSbO_3$ structure type. Magnetism and transport properties confirm that the system remains metallic for the entire solid solution. The combination of resistivity, susceptibility, and specific heat leads to this system of pyrochlores falling into a new class of Fermi liquids but with no obvious flat band effects.

Through this solid solution, Os has been shown to have a clear preference for adopting structures which allow for mixed valence and higher oxidation states. This first report on the novel Tl/Bi/Os oxide system allows for an initial understanding of the structure−property relationships of osmium compounds. Further work on the property characterization for osmium compounds can be done to bring clarity to the underlying mechanisms which drive the observed heat capacity and magnetic behavior.

ASSOCIATED CONTENT

Supporting Information

The Supporting Information is available free of charge at https://pubs.acs.org/doi/10.1021/acs.inorgchem.9b02939.

Raw neutron data for the $Tl_{2-x}Bi_xOs_2O_{7-y}$ samples (ZIP)

Additional XAS data on the $Tl_{2-x}Bi_xOs_2O_{7-y}$ samples and the Kadowaki−Woods plot and crystallographic information on the $Tl_{2-x}Bi_xOs_2O_{7-y}$ phases (PDF)

Accession Codes

CCDC 1957325−1957327 contain the supplementary crystallographic data for this paper. These data can be obtained free of charge via www.ccdc.cam.ac.uk/data_request/cif, or by

DOI: 10.1021/acs.inorgchem.9b02939
Inorg. Chem. 2020, 59, 1227−1233

emailing data_request@ccdc.cam.ac.uk, or by contacting The Cambridge Crystallographic Data Centre, 12 Union Road, Cambridge CB2 1EZ, UK; fax: +44 1223 336033.

AUTHOR INFORMATION

Corresponding Author

*E-mail for M.A.S.: Mas.Subramanian@oregonstate.edu.

ORCID

M. A. Subramanian: 0000-0001-5487-043X

Author Contributions

M.A.S. conceived the research interest. E.S.C. synthesized samples and ran high-temperature resistivity. E.S.C. and J.L. contributed to the structure refinements. D.H. ran all XAS measurements. A.P.R. and P.G.L. ran low-temperature resistivity and magnetism measurements. All authors contributed to the manuscript.

Notes

The authors declare no competing financial interest.

ACKNOWLEDGMENTS

This work was funded by the NSF grant DMR-1534711 (M.A.S.). Work at the Advanced Photon Source was supported by the U.S. Department of Energy (DOE), Office of Science, under Contract No. DE-AC02-06CH11357 (D.H.). A. P. Ramirez and P. G. LaBarre performed susceptibility and transport measurements below 300 K and were supported by Department of Energy Grant No. DE-SC0017862. The authors acknowledge Oak Ridge National Laboratory for providing access to their neutron facilities and helpful discussions when necessary. This research at ORNL's Spallation Neutron Source was sponsored by the Scientific User Facilities Division, Office of Basic Energy Sciences, U.S. Department of Energy.

REFERENCES

(1) Subramanian, M. A.; Aravamudan, G.; Subba Rao, G. V. Oxide Pyrochlores - A Review. *Prog. Solid State Chem.* **1983**, *15* (2), 55−143.

(2) Hanawa, M.; Muraoka, Y.; Tayama, T.; Sakakibara, T.; Yamaura, J.; Hiroi, Z. Superconductivity at 1 K in $Cd_2Re_2O_7$. *Phys. Rev. Lett.* **2001**, *87*, 187001.

(3) Yang, B.; Kim, Y. B. Topological Insulators and Metal-Insulator Transition in the Pyrochlore Iridates. *Phys. Rev. B: Condens. Matter Mater. Phys.* **2010**, *82* (82), 1−11.

(4) Sleight, A. W.; Gillson, J. L.; Weiher, J. F.; Bindloss, W. Semiconductor-Metal Transition In Novel $Cd_2Os_2O_7$. *Solid State Commun.* **1974**, *14*, 357−359.

(5) Wallace, M. K.; LaBarre, P. G.; Li, J.; Pi, S.-T.; Pickett, W. E.; Dessau, D. S.; Haskel, D.; Ramirez, A. P.; Subramanian, M. A. Local Moment Instability of Os in Honeycomb $Li_{2.15}Os_{0.85}O_3$. *Sci. Rep.* **2018**, *8*, 2−10.

(6) Shaplygin, I. S.; Lazarev, V. B. $Ln_2Os_2O_7$ - A New Family of Pyrochlores. *Mater. Res. Bull.* **1973**, *8* (12), 761−765.

(7) Sleight, A. W. New Ternary Oxides of Re, Os, Ir, and Pt with Cubic Crystal Structures. *Mater. Res. Bull.* **1974**, *9*, 1177−1184.

(8) Fujita, T.; Tsuchida, K.; Yasui, Y.; Kobayashi, Y.; Sato, M. Transport, Thermal and Magnetic Properties of $Bi_3Os_3O_{11}$ and $Bi_3Ru_3O_{11}$. *Phys. B* **2003**, *329-333*, 743−744.

(9) Yuan, Y.; Feng, H. L.; Shi, Y.; Tsujimoto, Y.; Belik, A. A.; Matsushita, Y.; Arai, M.; He, J.; Tanaka, M.; Yamaura, K. High-Pressure Synthesis, Crystal Structure, and Magnetic Properties of $KSbO_3$-Type 5*d* Oxides $K_{0.087}OsO_3$ and $Bi_{2.93}Os_3O_{11}$. *Sci. Technol. Adv. Mater.* **2014**, *15* (6), 064901.

(10) Giampaoli, G.; Li, J.; Ramirez, A. P.; Sleight, A. W.; Subramanian, M. A. $Bi_{2-x}Ca_xIr_2O_{6+y}$ Pyrochlore Phases: Structure and Properties with Varied Ir Oxidation State from 3.9+ to 4.3+. *Inorg. Chem.* **2017**, *56* (8), 4706−4715.

(11) Reading, J.; Knee, C. S.; Weller, M. T. Syntheses, Structures and Properties of Some Osmates (IV,V) Adopting the Pyrochlore and Weberite Structures. *J. Mater. Chem.* **2002**, *12*, 2376−2382.

(12) Sleight, A. W.; Gillson, J. L. Platinum Metal Pyrochlores ($T1_2M_2O_7$). *Mater. Res. Bull.* **1971**, *6* (1819), 781−784.

(13) Toby, B. H.; Toby, B. H.; Toby, B. H. EXPGUI, a Graphical User Interface for GSAS EXPGUI, a Graphical User Interface for GSAS. *J. Appl. Crystallogr.* **2001**, *34*, 210−213.

(14) Veiga, L. S. I.; Fabbris, G.; Veenendaal Van, M.; Feng, H. L.; Yamaura, K.; Haskel, D. Fragility of Ferromagnetic Double Exchange Interactions and Pressure Tuning of Magnetism in 3*d*-5*d* Double Perovskite Sr_2FeOsO_6. *Phys. Rev. B* **2015**, *91*, 235135.

(15) Shannon, R. D. Revised Effective Ionic Radii and Systematic Studies of Interatomic Distances in Halides and Chaleogenides. *Acta Crystallogr., Sect. A: Cryst. Phys., Diffr., Theor. Gen. Crystallogr.* **1976**, *32* (32), 751−767.

(16) Lee, K.-S.; Seo, D.-K.; Whangbo, M.-H. Structural and Electronic Factors Governing the Metallic and Nonmetallic Properties of the Pyrochlores $A_2Ru_2O_{7-y}$. *J. Solid State Chem.* **1997**, *131* (131), 405−408.

(17) Altermatt, D.; Brown, I. D. The Automatic Searching for Chemical Bonds in Inorganic Crystal Structures. *Acta Crystallogr., Sect. B: Struct. Sci.* **1985**, *B41*, 240−244.

(18) Shaplygin, I.S.; Lazarev, V.B. $CaOsO_3$ Decomposition Products: A New Orthorhombic Phase $Ca_2Os_2O_7$. *Thermochim. Acta* **1977**, *20*, 381−385.

(19) Shaplygin, I.S.; Lazarev, V.B. $CaOsO_3$ Decomposition Products: Condition Formation Of Defect Pyrochlores $Ca_2Os_2O_{7-x}$. *Thermochim. Acta* **1979**, *32*, 53−56.

(20) Shi, Q.; Snow, C. L.; Boerio-Goates, J.; Woodfield, B. F. Accurate Heat Capacity Measurements on Powdered Samples Using a Quantum Design Physical Property Measurement System. *J. Chem. Thermodyn.* **2010**, *42* (9), 1107−1115.

(21) Kadowaki, K.; Woods, S. B. Universal Relationship of the Resistivity and Specific Heat in Heavy-Fermion Compounds. *Solid State Commun.* **1986**, *58* (8), 507−509.

DOI: 10.1021/acs.inorgchem.9b02939
Inorg. Chem. 2020, 59, 1227−1233